Unified analysis of the sensitivities of reflectance and path length to scattering variations in a diffusive medium

Hanli Liu

A unified analysis is presented for the sensitivities of reflectance and path length to scattering variations in a diffusive medium, using an improved solution of the steady-state diffusion equation. This approach enables one to (1) explain theoretically two kinds of dependency of near-infrared reflectance on source–detector separations and (2) obtain an analytical expression for optical path lengths. The results shown here are consistent with those of Kumar and Schmitt [Appl. Opt. **36,** 2286 (1997)] and Mourant *et al.* [Appl. Opt. **36,** 5655 (1997)]. Also, discussions are given on (1) possible reasons for some inconsistency between the conclusion drawn by Mourant *et al.* and results given here and (2) the usefulness of making reflectance measurements while minimizing the sensitivity of reflectance and path length to scattering variations.

OCIS codes: 170.3660, 170.5280, 290.7050, 290.1990, 290.1350, 290.4210.

Recently, Kumar and Schmitt published a study on fiber spacing optimization for the least dependence of near-infrared (NIR) reflectance on changes in scattering properties, using an analytical solution of the diffusion equation with an empirically determined coefficient.[1] By taking the limit of large and small source–detector separations, ρ, they showed two opposite sensitivities of NIR reflectance to the reduced scattering coefficient (μ_s') and demonstrated that the sensitivity of the reflectance to μ_s' variations can be minimized for some value of ρ. Mourant *et al.* reported their computational and experimental evidence on a particular source–detector separation, at which the sensitivity of optical path lengths to μ_s' variations can be minimum.[2] In this paper a unified analysis is presented of the sensitivities of reflectance and path length to scattering variations in a diffusive medium with an improved solution of the steady-state diffusion equation. In this way we are able to explain theoretically two kinds of dependency of NIR reflectance on ρ and also demonstrate the correlations between the studies by Kumar and Schmitt[1] and by Mourant *et al.*[2] Moreover, this study will help with optimizing the measurement geometry and estimating optical path lengths in NIR spectroscopy (NIRS) studies.

In principle, diffusion theory can be employed to model light scattering and propagation in biological tissues only in the NIR range, where light scattering by tissues exists predominantly in comparison with light absorption. An improved solution for the steady-state diffuse reflectance with ρ larger than a few millimeters has been given by Kienle and Patterson, with an extrapolated boundary condition.[3] With refractive indices of $n_{\text{tissue}} = 1.4$ and $n_{\text{detector}} = 1$, a numerical aperture of 1 for the light-detection fiber, and a pencil beam as the incident light, the improved solution is written as

$$R_{\text{imp}}(\rho, z_0) = 0.118\Phi(\rho, z_0) + 0.306R(\rho, z_0), \quad (1)$$

where $\Phi(\rho, z_0)$ and $R(\rho, z_0)$ are the fluence rate and the z component of the photon flux across the tissue–air boundary, respectively, and they are given as

$$\Phi(\rho, z_0) = \frac{1}{4\pi D}\left[\frac{\exp(-\mu_{\text{eff}} r_1)}{r_1} - \frac{\exp(-\mu_{\text{eff}} r_2)}{r_2}\right], \quad (2)$$

$$R(\rho, z_0) = \frac{1}{4\pi}\left[z_0\left(\mu_{\text{eff}} + \frac{1}{r_1}\right)\frac{\exp(-\mu_{\text{eff}} r_1)}{r_1^2} + (z_0 + 4AD) \times \left(\mu_{\text{eff}} + \frac{1}{r_2}\right)\frac{\exp(-\mu_{\text{eff}} r_2)}{r_2^2}\right], \quad (3)$$

H. Liu (hanli@uta.edu) is with the Joint Program of Biomedical Engineering, The University of Texas at Arlington, UT Southwestern Medical Center, Arlington, Texas 76019.

Received 26 July 2000; revised manuscript received 14 December 2000.

0003-6935/01/101742-05$15.00/0

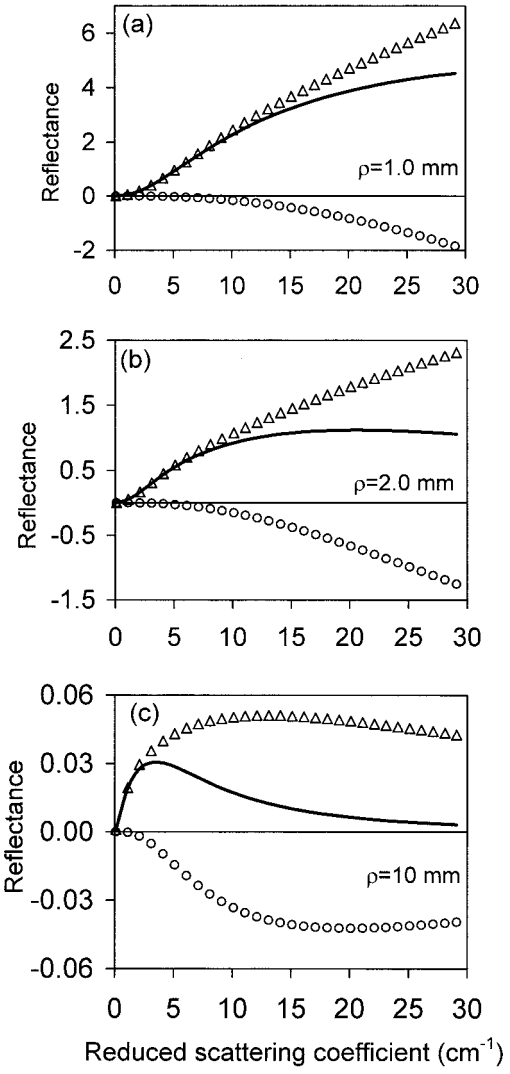

Fig. 1. Dependence of optical reflectance on μ_s', calculated with Eq. (1), at (a) $\rho = 1.0$ mm, (b) 2.0 mm, and (c) 10.0 mm with a fixed μ_a value of 0.1 cm^{-1}. The Y-axis unit is cm^{-2}. In each panel the curve plotted with triangles results from the isotropic light source at z_0, the curve with circles results from the virtual image source at z_0', and the solid curve is the summation of the other two curves that are due to the two different light sources.

and $r_1 = (z_0^2 + \rho^2)^{1/2}$, $r_2 = [(z_0 + 4AD)^2 + \rho^2]^{1/2}$, $\mu_{\text{eff}} = (\mu_a/D)^{1/2}$, $D = 1/3\mu_t'$ is the diffusion coefficient, $z_0 = 1/\mu_t'$ is the depth of the isotropic point source of the pencil beam, $\mu_t' = \mu_a + \mu_s'$, μ_a is the absorption coefficient, and A is a constant related to the internal reflection.[4] In the diffusion regime (i.e., $\mu_a \ll \mu_s'$), Eq. (1) is an improved solution with respect to Eq. (3), and both have shown to be in good agreement with spatially resolved Monte Carlo simulations with ρ larger than $\sim$2 mm.[3,4] For ρ equal to or smaller than 2 mm, Eq. (1) may not provide accurate results, since diffusion theory does not work well when the detector is too close to the light source. However, Eq. (1) may still be used to estimate and reveal primary patterns of light propagation in tissue.

It is known that the steady-state reflectance given in Eq. (1), R_{imp}, was derived by use of two light sources, an optical isotropic point source, located at z_0 below the surface of the measured medium, and its virtual image source located at $z_0' = -(z_0 + 2z_b)$, where z_b equals $2AD$ and is above the surface of the medium.[3,4] Comparisons between the total R_{imp} and the contributions from each light source calculated from Eq. (1) will help us understand better the relationship among R_{imp}, μ_s', and ρ for a given μ_a value. Figure 1 shows such a comparison of R_{imp} dependence on μ_s' at $\rho = 0.1$, 0.2, and 1.0 cm with a fixed μ_a value of 0.1 cm^{-1}. This figure demonstrates clearly that, when the separation is less than 0.2 cm (e.g., $\rho = 0.1$ cm), the total reflectance results mainly from the isotropic source at z_0 and increases monotonically as μ_s' increases. As the separation increases to 0.2 cm, the total R_{imp} becomes insensitive to μ_s' in the range of $\mu_s' > 8.0$ cm^{-1}. This is because the contribution from the isotropic source is balanced by that from the virtual image source, leading the total R_{imp} to a constant over a broad range of μ_s' (>8.0 cm^{-1}). However, as ρ keeps increasing (e.g., $\rho = 1.0$ cm), the contribution from the image source becomes more significant, making the total R_{imp} decrease as μ_s' increases in the range of $\mu_s' > 4$ cm^{-1}. Thus Eq. (1) along with Fig. 1 explains well that there exists an optimal source–detector separation, ρ_{opt}, at which the dependence of R_{imp} on tissue scattering property is minimum.

If taking the approach of Kumar and Schmitt,[1] we can define sensitivities of R to μ_s' and to μ_a (S_s and S_a) as

$$S_s = -\frac{\partial(\ln R_{\text{imp}})}{\partial \mu_s'}, \qquad S_a = -\frac{\partial(\ln R_{\text{imp}})}{\partial \mu_a},$$

respectively. After several mathematical manipulations from Eq. (1), we arrive at

$$S_s = -\frac{1}{R_{\text{imp}}}\frac{\partial R_{\text{imp}}}{\partial \mu_s'} = -\frac{1}{R_{\text{imp}}}(y_{\text{iso}} + y_{\text{ima}}), \qquad (4)$$

where y_{iso} and y_{ima} are two derivative components of R_{imp} with respect to μ_s' from the isotropic and image light source, respectively, and expressed as follows:

$$y_{\text{iso}} = \frac{\mu_t'}{4\pi {x_1}^2}\exp(-kx_1)\left[0.306\left(\frac{3}{{x_1}^3} + \frac{3k}{{x_1}^2} + \frac{k^2 - 1}{x_1} - k - \frac{k^2}{2}x_1\right) + 0.354\left(\frac{1}{x_1} + k + x_1 - \frac{k}{2}{x_1}^2\right)\right], \qquad (5)$$

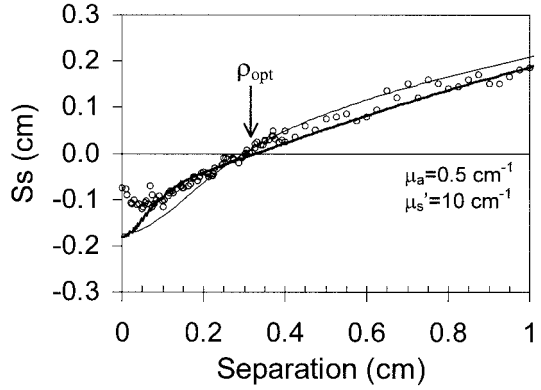

Fig. 2. Comparison of sensitivity of R with μ_s'. The thick curve was calculated with Eq. (4), the thin curve was obtained with the expression given by Kumar and Schmitt[1] with their empirically determined coefficient ($K = 2.5$), and the open circles were selectively replotted from the Monte Carlo simulations given by Kumar and Schmitt in Ref. 1. The absorption and reduced scattering coefficients used here are $\mu_a = 0.5$ cm^{-1} and $\mu_s' = 10$ cm^{-1}, respectively.

$$y_{\text{ima}} = \frac{\mu_t'}{4\pi x_2^2}\exp(-kx_2)\left[0.306\alpha\left(\frac{3\alpha^2}{x_2^3}+\frac{3k\alpha^2}{x_2^2}+\frac{k^2\alpha^2-1}{x_2}-k-\frac{k^2}{2}x_2\right)-0.354\left(\frac{\alpha^2}{x_2}+k\alpha^2+x_2-\frac{k}{2}x_2^2\right)\right], \tag{6}$$

where $x_1 = \mu_t' r_1$, $x_2 = \mu_t' r_2$, $k = z_0\mu_{\text{eff}} = (3\mu_a/\mu_t')^{1/2}$, and $\alpha = 4A/3 + 1$. With Eq. (4) we are able to calculate the sensitivity of R_{imp} to μ_s' at any given ρ with a chosen μ_a value. If we take the limit of large and small ρ, the results of S_s are consistent with those given by Kumar and Schmitt.[1] For direct comparison Fig. 2 shows two curves with $\mu_a = 0.5$ cm^{-1} and $\mu_s' = 10$ cm^{-1}, one curve calculated with Eq. (4) and the other obtained from the expression given by Kumar and Schmitt[1] with their empirically determined coefficient ($K = 2.5$). This figure shows clearly that S_s is negative if $\rho < \rho_{\text{opt}}$, zero if $\rho = \rho_{\text{opt}}$, and positive if $\rho > \rho_{\text{opt}}$. We have obtained $\rho_{\text{opt}} = 0.32$ cm in this case. Some of the Monte Carlo data given in Ref. 1 are also selectively replotted in this figure, illustrating that Eq. (4) matches the Monte Carlo simulations well, particularly at fiber separations greater than 1 mm. This consistency justifies the correctness of Eq. (4) to be used in the future to study S_s without dealing with any empirical parameters.

However, ρ_{opt} values are both μ_a and μ_s' dependent. To select an optimal separation at which S_s is near zero for a range of μ_a and μ_s', the dependence of S_s on both μ_s' and ρ at two different μ_a values was investigated. Figure 3 is a contour plot, comparing three constant-S_s curves with values of -0.02, 0.00, and 0.02 cm for cases of $\mu_a = 0.1$ and 0.5 cm^{-1}, respectively. It shows that the values of ρ_{opt} (along the contour curve of $S_s = 0.0$) are not constant,

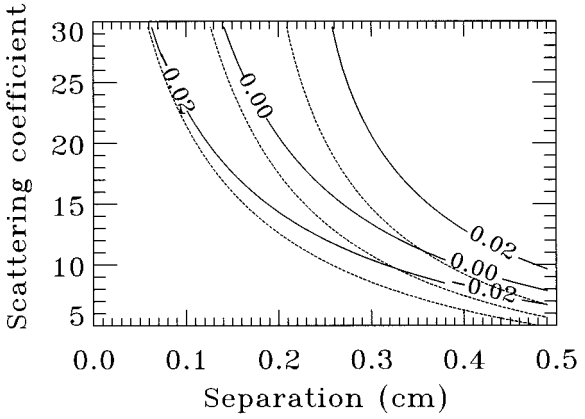

Fig. 3. Contour plot of sensitivity of R to μ_s', S_s, versus source–detector separation, ρ, and reduced scattering coefficient, μ_s', with $\mu_a = 0.1$ cm^{-1} (solid curves) and 0.5 cm^{-1} (dotted curves). The Y-axis unit is cm^{-1}. For both μ_a values the plotted contour curves have three constant values of S_s: -0.02, 0.00, and 0.02 cm. The dotted contour curves do not have labels because of space limitation, but they have the same varying tendency and pattern as the solid curves.

varying between 0.2 and 0.4 cm for a μ_s' range of 20–10 cm^{-1} with a fixed μ_a value of 0.1 cm^{-1}. When μ_a increases to 0.5 cm^{-1}, the ρ_{opt} values decrease and have a little weaker dependence on μ_s'. For example, ρ_{opt} changes from 0.18 to 0.32 cm as μ_s' decreases from 20 to 10 cm^{-1}. Although there exists no single optimal separation, ρ_{opt}, for a range of μ_s', e.g., 10–20 cm^{-1}, the variation of ρ_{opt} is relatively small, approximately a few millimeters, depending on both μ_s' and μ_a ranges of interest. Thus it is suggested to calculate an average of multiple ρ_{opt} values and use it as a unified optimal separation, ρ_{opt}', for actual separation selection. Further studies with multiple μ_a values (data not shown) have proved a general trend: A larger μ_a value results in a smaller range of ρ_{opt} variations for a given μ_s' range, allowing us to obtain a more accurate ρ_{opt}'.

Beer's law can be modified and used for calculations of optical reflectance from biological tissues, as written in Eq. (7),

$$R_{\text{imp}} = I_0\exp(-\mu_a L), \tag{7}$$

where I_0 is the incident light intensity per unit area, R_{imp} represents the collected diffuse reflectance, μ_a is the absorption coefficient of the medium (as defined above), and L is the optical path length traveled by photons through the tissue. For a chosen μ_a and constant I_0, Eq. (7) leads to Eq. (8),

$$L = S_a = -\frac{\partial \ln(R_{\text{imp}})}{\partial\mu_a} = -\frac{1}{R_{\text{imp}}}\frac{\partial R_{\text{imp}}}{\partial\mu_a} = \frac{1}{R_{\text{imp}}}(z_{\text{iso}} + z_{\text{ima}}), \tag{8}$$

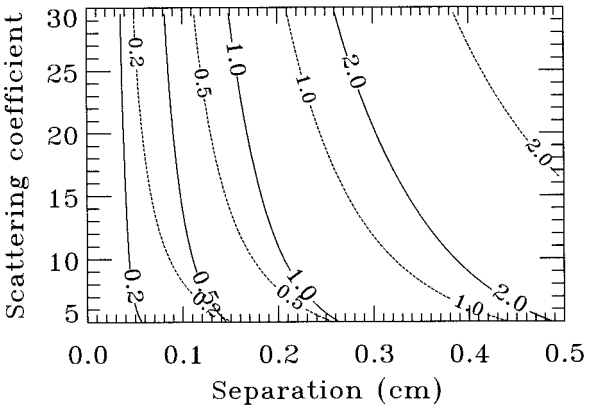

Fig. 4. Contour plot of optical pathlength, L, versus source–detector separation, ρ, and reduced scattering coefficient, μ_s', with $\mu_a = 0.1\ \mathrm{cm}^{-1}$ (solid curves) and $0.5\ \mathrm{cm}^{-1}$ (dotted curves). The Y-axis unit is cm^{-1}. For both μ_a values the plotted contour curves have four constant values of L: 0.2, 0.5, 1.0, and 2.0 cm.

where z_{iso} and z_{ima} are two derivative components of R_{imp} with respect to μ_a from the isotropic and image light source, respectively, and expressed as follows:

$$z_{\mathrm{iso}} = \frac{\mu_t'}{4\pi x_1^2}\exp(-kx_1)\left[0.306\left(\frac{3}{x_1^3}+\frac{3k}{x_1^2}+\frac{k^2-1}{x_1}-k-\frac{3}{2}x_1\right)+0.354\left(\frac{1}{x_1}+k+x_1-\frac{3}{2k}x_1^2\right)\right], \quad (9)$$

$$z_{\mathrm{ima}} = \frac{\mu_t'}{4\pi x_2^2}\exp(-kx_2)\left[0.306\alpha\left(\frac{3\alpha^2}{x_2^3}+\frac{3k\alpha^2}{x_2^2}+\frac{k^2\alpha^2-1}{x_2}-k-\frac{3}{2}x_2\right)-0.354\left(\frac{\alpha^2}{x_2}+k\alpha^2+x_2-\frac{3}{2k}x_2^2\right)\right]. \quad (10)$$

With Eq. (8) we are able to calculate the optical path length or the sensitivity of R_{imp} to μ_a at any given ρ for a chosen μ_a value. Figure 4 is a contour plot of optical path lengths, L, versus both ρ and μ_s', showing several constant-L curves with two μ_a values of 0.1 and $0.5\ \mathrm{cm}^{-1}$, respectively. It demonstrates that the variation of L is relatively small for both μ_a values in a μ_s' range of 10–30 cm^{-1} when ρ is equal to or less than 0.2 cm. A general trend that the dependence of L on μ_s' increases as ρ increases has been observed for other μ_a values.

An earlier study by Mourant *et al.*[2] showed that L appeared insensitive to μ_s' at an optimal source–detector separation, i.e., $\rho_{\mathrm{opt}}(L) = 1.7$ mm. To confirm their simulation results, they conducted experiments by taking optical spectra with and without a blue dye in aqueous suspensions of polystyrene spheres with different μ_s' values at wavelengths from 400 to 800 nm. The negative natural logarithms of the ratios between the spectra with and without the blue dye were taken. The areas, A, under the spectral curves from 575 to 595 nm were calculated and revealed to be dependent on the absorption coefficient of the added blue dye at 585 nm. Mathematically, based on Beer's law, these calculated areas could be expressed in the following way:

$$\begin{aligned}\mathrm{area} = A &= -\sum_{i=575\ \mathrm{nm}}^{595\ \mathrm{nm}} \ln\left[\frac{I(\lambda_i)}{I_0(\lambda_i)}\right] \\ &= \sum_{i=575\ \mathrm{nm}}^{595\ nm} \mathrm{O.D.}(\lambda_i) = \sum_{i=575\ \mathrm{nm}}^{595\ \mathrm{nm}} [\mu_a(\lambda_i)L_i(\lambda_i)] \\ &\cong k\,\mu_a(585\ \mathrm{nm})\langle L\rangle, \end{aligned} \quad (11)$$

where $I(\lambda_i)$ and $I_0(\lambda_i)$ represent the spectral intensities of the measured signal at wavelength λ_i with and without the blue dye, respectively; $\mathrm{O.D.}(\lambda_i)$ is optical density at wavelength λ_i and equal to $\mu_a(\lambda_i)L(\lambda_i)$; $\mu_a(585\ \mathrm{nm})$ and $\langle L\rangle$ are the absorption coefficient of the dye at 585 nm and a mean optical path length in the wavelength range of 575 to 595 nm, respectively, and k is a proportion constant. The final step in Eq. (11) is correct only if the μ_a values of the dye from 575 to 595 nm do not vary greatly. When Eq. (11) holds, a relative variation in A results in a relative variation in mean optical path length, $\langle L\rangle$. Thus Mourant *et al.*[2] determined percent variations in $\langle L\rangle$ approximately by measuring percent variations in A, showing that at an optimal source–detector separation, $\rho_{\mathrm{opt}}(L) = 1.7$ mm, percent variations in A, and thus in $\langle L\rangle$, are minimum, independent of scattering variations of the measured tissue phantoms.

In comparison, the analytical calculations plotted in Fig. 4 have a similar trend as that of the Monte Carlo data presented by Mourant *et al.* in Ref. 2. However, we do not observe a single optimal separation, $\rho_{\mathrm{opt}}(L)$, at only which the optical path length is insensitive to μ_s' variations. A possible reason for this inconsistency is as follows: The experimental quantity measured by Mourant *et al.*[2] was percent variations in area under the spectral curves. Although this quantity can be used to obtain an approximate mean optical path length, $\langle L\rangle$, based on Eq. (11), it is an average value of L over 575 to 595 nm. It is not accurate if the μ_a values of the blue dye in that spectral range are not exactly constant. Equation (8) calculates an exact optical path length at one particular wavelength. A further study to measure L at a single wavelength may be helpful to verify the correctness of Eq. (8) at $\rho \sim 0.2$–0.3 cm.

In spite of this inconsistency between Eq. (8) and the conclusion drawn by Mourant *et al.*[2] for small ρ values, it is believed that Eq. (8) is an accurate and useful expression to calculate optical path lengths when ρ is larger than 0.2–0.3 cm. This statement is supported by the consistency between the theoretical expressions, Eqs. (1) and (4), and Monte Carlo simulations, as shown in Fig. 7 of Ref. 3 and Fig. 2 of this paper, respectively. Previously,[1,5,6] when ρ is much larger than z_0, an optical path length has been approximately calculated as

$$L \approx \frac{\sqrt{3}}{2}\left(\frac{\mu_s'}{\mu_a}\right)^{1/2}\rho \qquad \text{if } \rho \gg z_0. \quad (12)$$

For Eq. (12) to be accurately valid for typical biological tissues, it usually requires $\rho = 3-4$ cm, i.e., approximately 30–40 times larger than z_0. If ρ has an intermediate or small value, i.e., $\rho < (5–20)z_0$, relation (12) does not hold well, whereas Eq. (8) can still give a relatively accurate result. This implies that Beer's law, with a modified optical path length as expressed in Eq. (8), can still be used correctly to analyze optical diffuse reflectance of tissues, as long as ρ is larger than a few millimeters.

The theoretical basis of this analysis is the diffusion approximation, and R_{imp} given in Eq. (1) has been derived from the fluence rate of NIR light propagating through tissues.[3] Since it is known that detailed behavior of the phase function may not be important for calculations of the fluence rate,[7] it is believed that the influence of the shape of the phase function on the results of S_s and L given above is minimum.

Noninvasive reflectance measurements for total hemoglobin concentration (Hb_t) and hemoglobin oxygen saturation (SO_2) in the brain,[6] muscle,[6] and tumors[8] are a few biomedical applications of NIRS. Recently, it has been reported that NIRS can be a useful, noninvasive tool in monitoring chemotherapy drug concentrations in tissue.[9] The measured endogenous or exogenous chromophores, such as Hb_t, SO_2, or chemotherapy drug concentrations, are highly light-absorption sensitive and can be quantified based on the NIRS measurement under different physiological conditions. However, scattering properties of tissues also vary and lead to large changes in reflectance signal when physiological conditions of the tissues are varied. It is desirable to make measurements under conditions in which the sensitivity of NIR reflectance to scattering changes is minimized. This will maximize the sensitivity of reflectance to the measured, absorption-sensitive, physiological parameters. Furthermore, if the sensitivity of optical path length to scattering changes is minimized, Eq. (7) can be used to calculate O.D. as conventional Beer's law:

$$\text{O.D.} = \mu_a L = \log(I_0/R_{\text{imp}}). \tag{13}$$

Since μ_a is equal to $\epsilon[c]$, where ϵ and $[c]$ are extinction coefficient and concentration of the measured chromophore, respectively, a simple relationship between two concentrations of the measured chromophore and two reflectance measurements exists:

$$\frac{[c]_1}{[c]_2} = \frac{\mu_a(1)}{\mu_a(2)} = \frac{\text{O.D.}(1)}{\text{O.D.}(2)} = \log\left[\frac{R_{\text{imp}}(2)}{R_{\text{imp}}(1)}\right], \tag{14}$$

where $R_{\text{imp}}(1)$ and $R_{\text{imp}}(2)$ denote two individual reflectance measurements from the tissue with two different concentrations, $[c]_1$ and $[c]_2$, respectively. Therefore minimizing the sensitivity of optical path length to scattering variations can significantly simplify concentration determinations for the measured chromophore, when multiple concentrations of the desired chromophore from the same tissue sample are required.

In summary, a unified analysis has been presented of sensitivities, S_s, of NIR reflectance and optical path lengths, L, to scattering variations with an improved solution of the steady-state diffusion equation. With this approach, we are theoretically able to (1) explain why, as scattering property of a measured medium increases, its optical reflectance increases with a small source–detector separation and decreases with a large separation; (2) investigate the dependency of optimal source–detector separation on both μ_s' and μ_a; and (3) obtain an analytical expression of optical path lengths for NIR reflectance, which can be a useful quantity when Beer's law is applied. This paper has demonstrated consistency with the results given by Kumar and Schmitt[1] and Mourant *et al.*[2] and also discussed possible reasons for some inconsistency with the conclusion drawn by Mourant *et al.*[2] Finally, discussion has been given on the usefulness of making practical measurements while minimizing the sensitivity of reflectance and optical path length to scattering variation.

The author acknowledges support from Whitaker Foundation research grant RG-97-0083.

References

1. G. Kumar and J. M. Schmitt, "Optimal probe geometry for near-infrared spectroscopy of biological tissue," Appl. Opt. **36,** 2286–2293 (1997).
2. J. R. Mourant, I. J. Bigio, D. A. Jack, T. M. Johnson, and H. D. Miller, "Measuring absorption coefficients in small volumes of highly scattering media: source–detector separations for which path lengths do not depend on scattering properties," Appl. Opt. **36,** 5655–5661 (1997).
3. A. Kienle and M. S. Patterson, "Improved solutions of the steady-state and the time-resolved diffusion equations for reflectance from a semi-infinite turbid medium," J. Opt. Soc. Am. A **14,** 246–254 (1997).
4. T. J. Farrell and M. S. Patterson, "A diffusion theory model of spatially resolved, steady-state diffuse reflectance for the noninvasive determination of tissue optical properties *in vivo*," Med. Phys. **19,** 879–888 (1992).
5. H. Liu, B. Beauvoit, M. Kimura, and B. Chance, "Dependence of tissue optical properties on solute-induced changes in refractive index and osmolarity," J. Biomed. Opt. **1,** 200–211 (1996).
6. E. M. Sevick, B. Chance, J. Leigh, S. Nioka, and M. Maris, "Quantitation of time- and frequency-resolved optical spectra for the determination of tissue oxygenation," Anal. Biochem. **195,** 330–351 (1991).
7. W. M. Star, "Diffusion theory of light transport," in *Optical-Thermal Response of Laser-Irradiated Tissue*, A. J. Welch and M. J. C. Van Gemert, eds. (Plenum, New York, 1995).
8. H. Liu, Y. Song, K. L. Worden, X. Jiang, A. Constantinescu, and R. P. Mason, "Noninvasive investigation of blood oxygenation dynamics of tumors by near-infrared spectroscopy," Appl. Opt. **39,** 5231–5243 (2000).
9. J. R. Mourant, T. M. Johnson, G. Los, and I. J. Bigio, "Noninvasive measurement of chemotherapy drug concentrations in tissue: preliminary demonstrations of *in vivo* measurements," Phys. Med. Biol. **44,** 1397–1417 (1999).